Experimental generation of entanglement-assisted quantum random access code

Xiao-Run Wang, Lu-Yan Wu, Chen-Xi Liu, Tong-Jun Liu, Jian Li,* and Qin Wang†

Institute of quantum information and technology, Nanjing University of Posts and Telecommunications, Nanjing 210003, China; Broadband Wireless Communication and Sensor Network Technology, Key Lab of Ministry of Education, NUPT, Nanjing 210003, China; and Telecommunication and Networks, National Engineering Research Center, NUPT, Nanjing 210003, China

(Received 25 January 2019; published 9 May 2019)

$n \to m$ random access code (RAC) is an information task to encode an n-bit random message into a shorter m-bit string. Resulting from the compression loss from n to m bits, there exists success probabilities for the string receiver to recover any bits of the initial message. It has been shown that success probabilities of bit recovery can be enhanced by employing quantum resources. Here we present experimental realizations of $2 \to 1$ and $3 \to 1$ distributed entanglement-assisted random access codes (EARACs) with a two-photon entangled source. The average success probabilities obtained in our experiment are 0.8491(41) for a $2 \to 1$ EARAC and 0.7724(34) for a $3 \to 1$ EARAC, exceeding the classical counterparts, respectively. Moreover, through the existing experimental data, success probabilities for n varying from 4 to 10 ($m = 1$) are estimated.

DOI: 10.1103/PhysRevA.99.052313

I. INTRODUCTION

Quantum resources have abundant advantages in the field of information processing, such as random access code (RAC) [1]. The classical $n \to m$ RAC is an information task to encode an n-bit random message into a shorter m-bit string, which is then sent to the receiver for recovering any bits of the initial message. By using quantum communication instead of classical communication, quantum random access code (QRAC) [2] delivers the initial message in a more accurate way. Nevertheless, QRAC allows only one bit of the initial message to be recovered each time because of the state collapse after measuring. The first work on QRAC was proposed by [3] named conjugate coding. Afterwards, Ambainis *et al.* show that there exists the scheme of $2 \to 1$ QRAC [1] and mention a generalization of $3 \to 1$ QRAC [4] (see [5] and [6] for more details). The $n \to m$ QRAC with $m > 1$ was researched in [1,4]. Moreover, $2 \to 1$ QRAC and $3 \to 1$ QRAC were realized experimentally in [7,8]. With the aid of high success probability, QRAC shows great application potential in the fields of network coding [5,9], locally decodable codes [10,11], quantum state learning [12,13], and quantum cryptography [14,15].

Entanglement-assisted random access code (EARAC) shares quantum entanglement among devices with a classical communication channel. In the case of a unit channel capacity, EARAC performs better than QRAC with classical shared randomness [8]. Moreover, Ref. [8] proposed a tripartite Bell-type inequality with the EARAC approach, which reveals that the protocol manifests genuine multipartite nonlocality. The other form of EARAC is distributed EARAC [16] with three components—preparation, transformation, and measurement devices. Furthermore, the use of a transformation device considerably improves noise tolerance when compared to simple prepare-and-measure networks [16].

Although it has been proved that QRAC does not exist without shared randomness (SR) when $n \geqslant 4$ [9], when parties are allowed to use SR, QRAC does exist for any n (see [2]). A general scenario can be constructed of $n \to m$ QRAC as well as EARAC by means of concatenation primitives that are $2 \to 1$ and $3 \to 1$ QRAC (EARAC). The fundamental distinction between EARAC and QRAC is that the encoding messages are hidden in the entanglement state shared among communicators rather than in a proper qubit. In the EARAC protocol, the process of communication between Alice, Bob, and Charlie is completed by measuring each qubit on their part, while in the QRAC protocol, Alice needs to prepare a proper state then transmits it to Bob to measure. When there are strong noises in the quantum channel, the prepared state in the QRAC will be affected, thus affecting the ultimate measurement result. Nevertheless, the measurement results will not be influenced in the EARAC because the purity of the entanglement state can be improved by means of entanglement purification.

Here, we report experimental realizations of $2 \to 1$ and $3 \to 1$ distributed EARAC [8,17] using the photonics system. The average success probability obtained in our experiment exceeds the optimal classical bound and fits well with corresponding theoretical probability, verifying the advantages of quantum resource over classical ones. Furthermore, we calculate the success probability for a general scenario $n \to 1$ EARAC when n varies from 4 to 10.

II. $2 \to 1$ AND $3 \to 1$ EARAC

In the $2 \to 1$ EARAC, a maximally entangled state $|\psi\rangle = \frac{1}{\sqrt{2}}(|00\rangle + |11\rangle)$ is shared between Alice and Bob. Alice encodes two bits $x_0, x_1 \in \{0, 1\}$ by performing measurements on one side of the Bell state in the basis of

$$M_A^a = \tfrac{1}{2}\big(I + \vec{A}_x^a \cdot \vec{\sigma}\big), \tag{1}$$

*jianli@njupt.edu.cn
†qinw@njupt.edu.cn

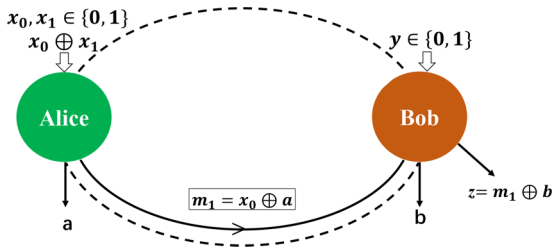

FIG. 1. Simple network of $2 \to 1$ EARAC. The dotted line indicates the entangled state shared between Alice and Bob as well as the solid line corresponds to the classical communication channel between them. Classical bits x_0, x_1 are initial encoding bits and the result of $x_0 \oplus x_1$ decides the specific measurement in Alice's side. The decoding device receives an input $y \in \{0, 1\}$ with an aim to guess x_y in higher success probability. The auxiliary bit $m_1 = x_0 \oplus a$ is transmitted in classical channel between Alice and Bob.

where $A_x^a = (-1)^a \cdot \vec{a}, \vec{a} = (\frac{1}{\sqrt{2}}, \frac{(-1)^x}{\sqrt{2}}, 0)$ and $x = x_0 \oplus x_1$. The measurement outcome of Alice is represented as $a \in \{0, 1\}$. After Alice's measurement, she delivers one classical bit denoted as $m_1 = x_0 \oplus a$ to Bob. (as shown in Fig. 1). Note that the auxiliary classical bit m_1 is neither a determinate message nor a function of original classical bits x_0, x_1. Bob receives an input $y \in \{0, 1\}$ with an aim to guess x_y by measuring the other side of the Bell state in the basis

$$M_B^b = \tfrac{1}{2}\big(I + \vec{B}_y^b \cdot \vec{\sigma}\big), \tag{2}$$

where $B_y^b = (-1)^b \cdot \vec{b}, \vec{b} = (1, 0, 0)$ or $\vec{b} = (0, 1, 0)$ and $b \in \{0, 1\}$. Bob's guess for x_y is $m_1 \oplus b$. The output $z = x_y$ is a function of x, y and the success probability can be described as $p(z = f(x, y)|x, y)$. Eventually, the success probability p can be calculated by

$$p(m \oplus b = x_y) = \tfrac{1}{2}(1 + \vec{a} \cdot \vec{b}). \tag{3}$$

Therefore, the theoretical success probability in $2 \to 1$ EARAC is $p = \frac{1}{2}(1 + \frac{1}{\sqrt{2}})$. In the course of experiment, the average success probability can be calculated by

$$P = \frac{1}{8} \sum p(z = f(x, y)|x, y), \tag{4}$$

where $p(z = f(x, y)|x, y)$ is the success probability for each bit. The average success probability of guessing x_y is $\frac{3}{4}$ in $2 \to 1$ RAC for a classical system.

The standard $3 \to 1$ RAC is a communication complexity problem defined in a prepare and measure scenario. An experimental demonstration of $3 \to 1$ distributed QRAC was presented in [8], which adopted a single-photon source. Both $3 \to 1$ QRAC and EARAC offer the same success probability $P = \frac{1+\sqrt{3}}{2\sqrt{3}} \approx 0.7887$ [1,17]. In the network of a distributed EARAC (as shown in Fig. 2), the preparation device is split into two parts (Alice and Bob) such that Alice receives two bits x_0, x_1 and Bob receives only one bit x_2. The task of the decoding part (Charlie) is to decode the initial string in higher success probability. Alice, Bob, and Charlie share a three-qubit Greenberger-Horne-Zeilinger state in the form of

$$|\varphi\rangle = \frac{1}{\sqrt{2}}(|000\rangle + |111\rangle). \tag{5}$$

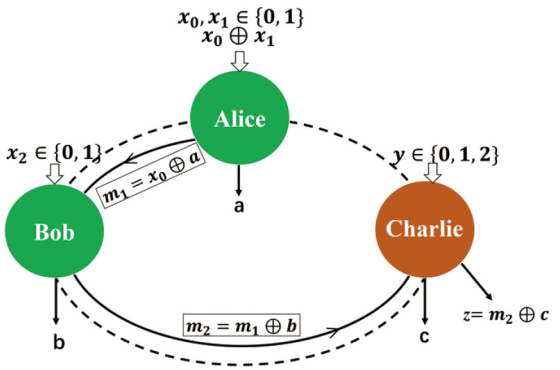

FIG. 2. Experimental model of $3 \to 1$ entanglement-assisted distributed random access code. The solid line indicates the entangled state shared between Alice and Bob as well as the dotted line corresponds to the classical communication channel between them. Three classical bits x_0, x_1, x_2 (where $x_i \in \{0, 1\}$) are split into two parts x_0, x_1 and x_2. Alice encodes the first two bits in her measurements and Bob encodes the last bit in his measurement basis. Charlie's input $y \in \{0, 1, 2\}$ determines different measurements on his party.

By performing different measurements on their qubits, Alice and Bob complete the process of encoding. Alice encodes first two bits x_0, x_1 with her measurements

$$M_A^a = \tfrac{1}{2}\big(I + \vec{A}_x^a \cdot \vec{\sigma}\big), \tag{6}$$

where $A_x^a = (-1)^a \cdot (\frac{1}{\sqrt{2}}, \frac{(-1)^{x+1}}{\sqrt{2}}, 0)$ and $x = x_0 \oplus x_1$ as well as gives out a measurement output $a \in \{0, 1\}$. Afterwards, she transmits one bit $m_1 = x_0 \oplus a$ to Bob who encodes the last bit x_2 and m_1 into his measurements and provides an output $b \in \{0, 1\}$. Bob's bases are as follows:

$$M_B^b = \tfrac{1}{2}\big(I + \vec{B}_{mx}^b \cdot \vec{\sigma}\big), \tag{7}$$

where $B_0 = (\cos 2\theta, 0, \sin 2\theta)$, $B_1 = (-\cos 2\theta, 0, -\sin 2\theta)$, and

$$\theta = \cos^{-1}\left(\sqrt{\frac{\sqrt{3} + (-1)^{m_1 \oplus x_2}}{2\sqrt{3}}}\right)$$

Subsequently, Bob sends the final encoding bit $m_2 = m_1 \oplus b$ to Charlie. Note that auxiliary classical bits m_1, m_2 are neither a determinate message nor a function of original classical bits x_0, x_1, x_2. Charlie uses a set of orthogonal complete bases such as $\sigma_y, \sigma_x, \sigma_z$ to measure the particle in his party according to different bits he want to acquire in initial string and obtain an output $c \in \{0, 1\}$. Furthermore, Charlie combines his measured output c and a received bit m_2 to realize the decoding process of the original bit string. Charlie's guess for x_y is $m_2 \oplus c$. The output $z = x_y$ is a function of x, y as well as the success probability can be described as $p(z = f(x, y)|x, y)$. The average success probability is calculated by

$$P = \frac{1}{24} \sum p(z = f(x, y)|x, y). \tag{8}$$

By considering all classical deterministic strategies, it can be checked that when $f(x, 0), f(x, 1), f(x, 2)$ are independent of each other, then the upper bound of P using a classical channel is $\frac{2}{3}$.

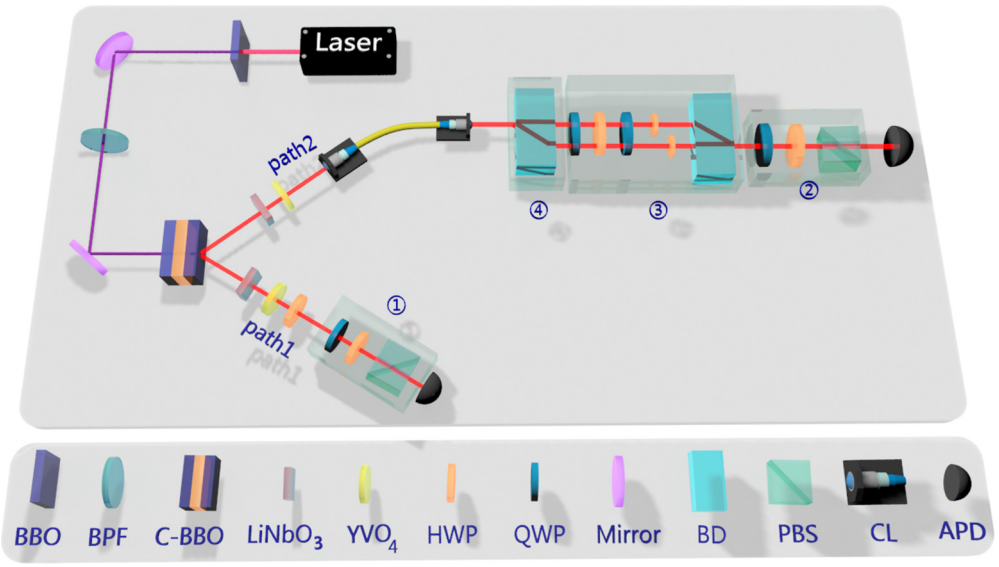

FIG. 3. Experimental setup for implementing $2 \to 1$ and $3 \to 1$ distributed entanglement-assisted random access code. In the state preparation process, a pair of entangled photons is first generated via a type-II phase matching β-barium-borate crystal. The first photon of each pair then passes through beam displacers to generate a pair of qubits, encoded in its path, and polarization degrees of freedom, while the polarization of the second photon encodes a third qubit. The boxes 1 and 2 are measurement setups of Alice and Bob in the $2 \to 1$ EARAC. The boxes 3 and 2 and 1 are measurement setups of Alice, Bob, and Charlie in the $3 \to 1$ EARAC. BBO: a β-barium-borate (BBO) crystal cut for collinear type-I phase matching; C-BBO: sandwich-type BBO+HWP+BBO combination; QWP: quarter-wave plate; HWP: half-wave plate; PBS: polarzing beam splitter; BD: calcite beam displacer; APD: single-photon detector.

III. EXPERIMENTAL DETAILS AND RESULTS

The experimental setup to realize $2 \to 1$ and $3 \to 1$ EARAC is shown in Fig. 3, which includes state preparation and measurement. Let us begin with a $2 \to 1$ EARAC scenario first. In order to carry on an experimental realization of the $2 \to 1$ EARAC, we first prepare a two-photon polarization-entangled state by the process of spontaneous parametric down-conversion (SPDC). A mode-locked Ti:sapphire pulsed laser (with a duration of less than 100 fs, a repetition rate of 80 MHz, and a central wavelength of 780 nm) is frequency doubled into 390 nm by a type-I phase-matching β-barium-borate (BBO) crystal, then focused onto the sandwich-type down-converter composed of two β-BBO crystals cut for beamlike type-II phase matching with a true-zero-order half-wavelength plate between them (see more details in [18–20]). The maximally entangled state, $|\phi^+\rangle = \frac{1}{\sqrt{2}}(|HH\rangle + |VV\rangle)$, is generated. The photon 1 and photon 2 are two qubit generated in path 1 and path 2, respectively. The source provided on average 1300 coincidences per second. We perform quantum state tomography on the generated state and the fidelity is up to $98.45 \pm 0.22\%$.

The $2 \to 1$ EARAC for Alice and Bob, who share the two entangled photons, can be realized where Alice and Bob perform the measurement on photons 1 and 2, respectively. In the process of $2 \to 1$ EARAC, we use the setup in the boxes 1 and 2 individually, while boxes 3 and 4 are not included (shown in Fig. 3). Alice encodes her two classical bits into her measurement on the polarization degree of freedom of photon 1 by using a combination of half-wave plate (HWP), quarter-wave plate (QWP), and polarized beam splitter (PBS) shown in the box 1 of Fig. 3. Similarly, Bob selects an appropriate basis acting on polarization degree of freedom of photon 2 according to the initial bits he wants to recover (shown in the box 2 of Fig. 3). Specific settings of wave plates are listed in the Appendix to realize the measurements in Eqs. (1) and (2). Moreover, we used silicon avalanche photodiodes (APDs) to detect photon coincidences at output ports of two PBS. For each set of measurements, the time intervals of data acquisition are set to 10 s. Success probabilities in this part are presented in Table I. The average success probability is 0.8491(41), which is adjacent to theoretical probability.

As for a $3 \to 1$ EARAC, three-qubit GHZ state is shared among Alice, Bob, and Charlie. In experiment, we prepared three-qubit states based on the photon pair described by $|\phi^+\rangle$. The polarization degrees of freedom of the photon pair encode two qubits, labeled as B and C, respectively. As shown in the box 4 of Fig. 3, the photon 2 is sent through the first calcite beam displacer (BD) which acts such that the vertically polarized component of the first photon passes into the upper path, while the horizontally polarized component passes into the lower path. Thus the first BD entangles the path and polarization degrees of freedom of photon 2. This path degree of freedom of the photon 2 encodes a qubit labeled as A. Along with the qubit B and qubit C, the state preparation process

TABLE I. Success probability in $2 \to 1$ EARAC. The averaged probability is 0.8491(41) adjacent to theoretical probability.

x_0x_1	$p(x_0)$	$p(x_1)$	$p(x_0x_1)$
00	0.8528(41)	0.8545(40)	0.8537(41)
01	0.8356(40)	0.8688(43)	0.8612(42)
10	0.8537(42)	0.8184(38)	0.8361(40)
11	0.8592(42)	0.8318(40)	0.8455(41)

TABLE II. Success probability of eight different strings of $3 \to 1$ EARAC. The averaged probability is 0.7724(34) adjacent to theoretical probability.

$x_0x_1x_2$	$P(x_0)$	$P(x_0)$	$P(x_0)$	$P(x_0x_1x_2)$
000	0.7573(33)	0.7958(36)	0.7446(33)	0.7659(34)
001	0.7479(32)	0.7390(33)	0.8204(37)	0.7691(34)
010	0.8069(36)	0.7242(32)	0.7883(35)	0.7731(34)
011	0.7833(35)	0.7842(35)	0.7731(34)	0.7802(34)
100	0.7786(35)	0.7750(35)	0.7704(34)	0.7747(34)
101	0.8110(37)	0.7306(31)	0.7886(35)	0.7767(34)
110	0.7437(33)	0.7520(33)	0.8214(37)	0.7724(34)
111	0.7441(33)	0.8124(37)	0.7440(32)	0.7668(34)

generates entangled three-qubit states. The qubit A of Alice corresponds to path information of photon 2. Likewise, the qubit B of Bob and the qubit C of Charlie correspond to the polarization of photon 2 and photon 1, respectively.

At the stage of state measurement, Alice's and Bob's measurements are realized as shown in the boxes 3 and 2 of Fig. 3, respectively, as well as Charlie's measurements are realized in the box 1. Alice adopts a combination of half-wave plate [HWP (φ)] and two quarter-wave plates (both $\theta = 45^\circ$ with its fast axis) to ensure the suitable phase in her measurements. In addition, two different HWPs, forming an angle of -22.5° and 22.5° with its fast axis, respectively, locate at different ways before the second BD to ensure the appropriate amplitude for Alice's basis. After the measurements of Alice, the path information corresponding to qubit A converts to polarization states. Furthermore, Alice transmits a classical bit $m_1 = x_0 \oplus a$ to Bob. Bob's basis to measure the qubit B is shown in Eq. (7), which not only depends on his own bit x_2 but also on bit m_1 received from Alice. It can be realizable to array a HWP, a QWP, and a PBS in sequence. As for Charlie, his task is to measure the qubit C (the polarization of photon 1) in $\sigma_y, \sigma_x, \sigma_z$ and thus recover the initial bit in a higher success probability. Furthermore, he utilizes his own measurement output c and an auxiliary bit m_2 from Bob to recover the desired bit in a success probability. Similarly, Charlie's measurements are made up of one HWP, one QWP, and one PBS. All degrees of three basis are listed in the Appendix.

Furthermore, we also used silicon avalanche photodiodes (APDs) to detect photon coincidences at output ports of two PBS. For each set of measurements, the time intervals of data acquisition are set to 10 s. The success probabilities for $3 \to 1$ distributed EARAC are presented in Table II. The final success probability in our experiment is 0.7724(34), which is close to the theoretical probability of $\frac{1}{2}(1 + \frac{1}{\sqrt{3}})$.

IV. CONCATENATION

An $n \to 1$ EARAC can be realized by concatenating the $2 \to 1$ and (or) the $3 \to 1$ EARAC [17]. For example, the $4 \to 1$ EARAC can be performed by three $2 \to 1$ ones (shown in Fig. 4). The initial bit string x_0, x_1, x_2, x_3 can be divided into two parts. For every part, the same process of $2 \to 1$ EARAC is performed. In the same way, with regards to the output of the aforementioned two parts, the third

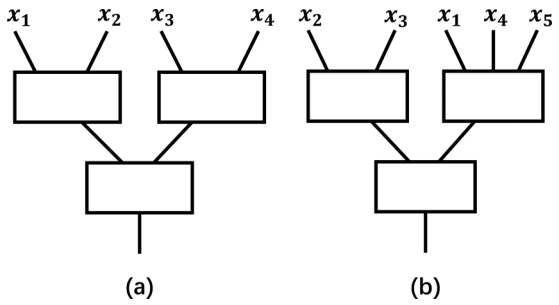

FIG. 4. Examples of two possible concatenation for $5 \to 1$ EARAC. The probability of Bob guessing x_2 is higher than for x_3 since the success probability in $2 \to 1$ EARAC is higher than $3 \to 1$ EARAC. The success probability for guessing x_2 and x_3 is $P_2 = \frac{1}{2}(1 + \frac{1}{\sqrt{4}})(k = 2, j = 0)$ and $P_3 = \frac{1}{2}(1 + \frac{1}{\sqrt{6}})(k = 1, j = 1)$, respectively. Therefore, the averaged success probability is $p = \frac{2}{5}P_2 + \frac{3}{5}P_3$.

$2 \to 1$ EARAC is executed so that we get the final success probability for $n = 4$. In $5 \to 1$ EARAC, there are different permutations of input bits. One possible permutation of input bits is shown in Fig. 4. More generally, for any n, one can divide them into n_2 groups of 2 and n_3 groups of 3 to get the final success probability by adopting the similar way aforementioned. For a specific bit in the bit string, the success probability depends on which position is located since the success probability in $n = 2$ is higher than $n = 3$. Therefore, the final probability should be averaged. In conclusion, the final success probability not only depends on the primitives in every step, but also the numbers of the correct and incorrect steps.

In the process of concatenation $2 \to 1$ and $3 \to 1$ EARAC, the success probability can be written as Eq. (9) when the number of inaccurate steps is even:

$$p_{2e}(k) = \tfrac{1}{2}\left(1 + 2^{-\frac{k}{2}}\right), \quad p_{3e}(k) = \tfrac{1}{2}\left(1 + 3^{-\frac{k}{2}}\right). \tag{9}$$

Likewise, for an odd number of errors [17], one has

$$p_{2o}(k) = \tfrac{1}{2}\left(1 - 2^{-\frac{k}{2}}\right), \quad p_{3o}(k) = \tfrac{1}{2}\left(1 - 3^{-\frac{k}{2}}\right). \tag{10}$$

As a result, the total probability [17] for receiver is written as

$$\begin{aligned} p(k, j) &= p_{2e}(k)p_{3e}(k) + p_{2o}(k)p_{3o}(k) \\ &= \tfrac{1}{2}\left(1 + 2^{-\frac{k}{2}}3^{-\frac{j}{2}}\right). \end{aligned} \tag{11}$$

TABLE III. Success probability for a $(n, 1, p_n)$ EARAC compared theoretical probability with an experimentally possible one.

n	p_n^T	p_n^E
4	$\frac{3}{4}$	0.7437(57)
5	$\frac{1}{20}(12 + \sqrt{6})$	0.7117(50)
6	$\frac{1}{2}(1 + \frac{1}{\sqrt{6}})$	0.6902(46)
7	$\frac{1}{21}(12 + \sqrt{6})$	0.6723(42)
8	$\frac{1}{80}(52 + \sqrt{6})$	0.6702(60)
9	$\frac{2}{3}$	0.6589(39)
10	$\frac{1}{20}(10 + \sqrt{2} + \sqrt{3})$	0.6473(58)

It is worth noticing that whatever the size of n is, the final success probability will exceed $\frac{1}{2}$ according to Eq. (11). Taking advantage of our experimental result in $2 \to 1$ and $3 \to 1$ EARACs and Eq. (11), we calculate several cases from $n = 4$ to $n = 10$ listed in Table III.

V. CONCLUSIONS

We have experimentally implemented a $2 \to 1$ as well as a $3 \to 1$ EARAC with success probabilities 0.8491(41) and 0.7724(34), respectively, by adopting a Bell state. Originally, we just employ a Bell state and a combination of wave plates to realize the process of encoding and decoding in a $2 \to 1$ EARAC. What is more, in a $3 \to 1$ EARAC, we construct an interferometer consisting of two BDs on the basis of a Bell state for the sake of completing the preparation of GHZ state. With the comparison of classical RACs and heralded single-photon source based QRACs, our EARACs show distinct advantages both in the success probability and without shared randomness. Therefore, our present work can provide valuable references for further implementation of EARACs into quantum information and quantum dense coding. Last but not least, taking advantage of a combination of the $2 \to 1$ EARAC and (or) the $3 \to 1$ EARAC can realize $n \to 1$ EARAC [17]. We present success probabilities of two cases and calculate several examples from $n = 4$ to $n = 10$ based on concatenation, comparing with corresponding theoretical ones.

In fact, we did not apply electrical-modulated optical (EOM) devices in our experiment, but carried out corresponding operations manually. In practical application, in order to encode a random bit in real-time scenarios, the EOM devices should be applied to real-time control Bob's (Charlie's) measurement basis according to Alice's measurement results. Therefore, this is just a proof-of-principle demonstration.

In addition, there are some noises and imperfections in our system. For example, the entanglement and fidelity of two-photon entangled states are $98.73 \pm 0.27\%$ and $98.45 \pm 0.22\%$, respectively, which are not the maximum entangled two-qubit states. Besides, the interference visibility of the BD interferometer is $98.58 \pm 0.35\%$, which is not the perfect interference. Those imperfections will influence converting path information to polarization information executed by Alice, and further result in slight deviations between experimental data and theoretical predictions.

ACKNOWLEDGMENTS

We acknowledge the financial support by the National Key R&D Program of China (Grants No. 2018YFA0306400 and No. 2017YFA0304100), the National Natural Science Foundation of China (Grants No. 61475197, No. 11774180, and No. 61590932), and the Postgraduate Research and Practice Innovation Program of Jiangsu Province (Grant No. KYCX18-0915).

TABLE IV. Specific settings of wave plates are demonstrated to realize the measurements in Eq. (1) and Eq. (2) in $2 \to 1$ EARAC.

Alice's measurement			
Case	Output	$\frac{1}{2}\lambda$	$\frac{1}{4}\lambda$
$x_0 \oplus x_1 = 0$	$a = 0$	146.25°	135°
	$a = 1$	33.75°	45°
$x_0 \oplus x_1 = 1$	$a = 0$	56.25°	45°
	$a = 1$	11.25°	45°
Bob's measurement			
Case	Output	$\frac{1}{2}\lambda$	$\frac{1}{4}\lambda$
$y = 0$	$b = 0$	22.5°	45°
	$b = 1$	−22.5°	45°
$y = 1$	$b = 0$	0°	45°
	$b = 1$	0°	−45°

APPENDIX

Here we provide specific settings of wave plates in $2 \to 1$ (Table IV) and $3 \to 1$ (Table V) EARAC to encode and decode the classical bit string. Note that all degrees are forming with their fast axis.

TABLE V. Orientation of combined wave plates allows Alice, Bob, and Charlie to complete the process of encoding and decoding in $3 \to 1$ EARAC.

Alice's measurement			
Case	Output	φ	θ
$x_0 \oplus x_1 = 0$	$a = 0$	56.25°	45°
	$a = 1$	11.25°	45°
$x_0 \oplus x_1 = 1$	$a = 0$	78.75°	45°
	$a = 1$	33.75°	45°
Bob's measurement			
Case	Output	$\frac{1}{2}\lambda$	$\frac{1}{4}\lambda$
$m_1 \oplus x_2 = 0$	$b = 0$	13.68°	180°
	$b = 1$	58.68°	90°
$m_1 \oplus x_2 = 1$	$b = 0$	31.32°	180°
	$b = 1$	166.32°	0°
Charlie's measurement			
Case	Output	$\frac{1}{2}\lambda$	$\frac{1}{4}\lambda$
$y = 0$	$c = 0$	0°	135°
	$c = 1$	0°	45°
$y = 1$	$c = 0$	22.5°	0°
	$c = 1$	67.5°	90°
$y = 2$	$c = 0$	0°	0°
	$c = 1$	45°	0°

[1] A. Ambainis, A. Nayak, A. Ta-Shama, and U. Varizani, in *Proceedings of 31st ACM Symposium on Theory of Computing* (ACM, New York, 1999), pp. 376–383; J. Assoc. Comput. Mach. **49**, 496 (2002).

[2] A. Ambainis, D. Leung, L. Mancinska, and M. Ozols, arXiv:0810.2937.

[3] S. Wiesner, SIGACT News **15**, 78 (1983).

[4] A. Nayak, in *Proceedings of the 40th IEEE Symposium on Foundations of Computer Science (FOCS'99)* (IEEE Computer Society, Washington, DC, 1999), pp. 369–376.

[5] M. Hayashi, K. Iwama, H. Nishimura, R. Raymond, and S. Yamashita, New J. Phys. **8**, 129 (2006).

[6] A. Casaccino, E. F. Galvão, and S. Severini, Phys. Rev. A **78**, 022310 (2008).

[7] R. W. Spekkens, D. H. Buzacott, A. J. Keehn, B. Toner, and G. J. Pryde, Phys. Rev. Lett. **102**, 010401 (2009).

[8] A. Hameedi, D. Saha, P. Mironowicz, M. Pawłowski, and M. Bourennane, Phys. Rev. A **95**, 052345 (2017).

[9] M. Hayashi, K. Iwama, H. Nishimura, R. Raymond, and S. Yamashita, in *Quantum Network Coding*, edited by W. Thomas and P. Weil, Lecture Notes in Computer Science (STACS 2007 SE52 Vol. 4393) (Springer, Berlin, 2007).

[10] I. Kerenidis, Ph.D. thesis, University of California at Berkeley, 2004.

[11] I. Kerenidis and R. de Wolf, J. Comput. Syst. Sci. **69**, 395 (2004).

[12] S. Aaronson, Proc. R. Soc. A **463**, 3089 (2007).

[13] S. Yu, F. Albarran-Arriagada, J. C. Retamal *et al.*, Adv. Quantum Technol. **2**, 1800074 (2019).

[14] C. H. Zhang, X. Y. Zhou, H. J. Ding, C. M. Zhang, G. C. Guo, and Q. Wang, Phys. Rev. Appl. **10**, 034033 (2018).

[15] H. W. Li, M. Pawłowski, Z. Q. Yin, G. C. Guo, and Z. F. Han, Phys. Rev. A **85**, 052308 (2012).

[16] J. Bowles, N. Brunner, and M. Pawłowski, Phys. Rev. A **92**, 022351 (2015).

[17] M. Pawłowski and M. Żukowski, Phys. Rev. A **81**, 042326 (2010).

[18] C. Zhang, Y.-F. Huang, Z. Wang, B.-H. Liu, C.-F. Li, and G.-C. Guo, Phys. Rev. Lett. **115**, 260402 (2015).

[19] T. J. Liu, C. Y. Wang, J. Li, and Q. Wang, Europhys. Lett. **119**, 14002 (2017).

[20] J. Li, C. Y. Wang, T. J. Liu, and Q. Wang, Phys. Rev. A **97**, 032107 (2018).